RESEARCH ARTICLE
PLANETARY SCIENCES

Earth and Planetary Physics
8: 307–316, 2024
doi: 10.26464/epp2024002

Thermosphere joint observations by TM-1 constellations and Swarm-B during the April 2023 geomagnetic storm

YongPing Li[1,2,3,4*], YueQiang Sun[1,2,3,4], XianGuo Zhang[1,2,3,4], JiangZhao Ai[1,2,3], XiaoLiang Zheng[1,2,3], Jia Li[1,2,3], YuJie Wang[1,2,3], BiBo Guo[5], Feng Yan[5], ShiLong Wei[5], XinChun Tang[5], and YuanYuan Cao[5]

[1]National Space Science Center, Chinese Academy of Sciences, Beijing 100190, China;

[2]Beijing Key Laboratory of Space Environment Exploration, Beijing 100190, China;

[3]Key Laboratory of Science and Technology on Space Environment Situational Awareness, Chinese Academy of Sciences, Beijing 100190, China;

[4]University of Chinese Academy of Sciences, Beijing 100049, China;

[5]Shenzhen Aerospace Dongfanghong Satellite, Ltd, Shenzhen 518057, China

Key Points:

- We present the first joint observations of thermosphere density observed by the TM-1 constellation during a geomagnetic storm.
- The TM-1 mass density data are compared with ESA's Swarm-B data and NRLMSISE00 simulations.
- Response of thermosphere mass density at multiple different Local Times during the geomagnetic storm.

Citation: Li, Y. P., Sun, Y. Q., Zhang, X. G., Ai, J. Z., Zheng, X. L., Li, J., Wang, Y. J., Guo, B. B., Yan, F., Wei, S. L., Tang, X. C., and Cao, Y. Y. (2024). Thermosphere joint observations by TM-1 constellations and Swarm-B during the April 2023 geomagnetic storm. *Earth Planet. Phys.*, *8*(2), 307–316. http://doi.org/10.26464/epp2024002

Abstract: The response of thermosphere density to geomagnetic storms is a complicated physical process. Multi-satellite joint observations at the same altitude but different local times (LTs) are important for understanding this process; however, until now such studies have hardly been done. In this report, we analyze in detail the thermosphere mass density response at 510 km during the April 23–24, 2023 geomagnetic storm using data derived from the TM-1 (TianMu-1) satellite constellation and Swarm-B satellites. The observations show that there were significant LT differences in the hemispheric asymmetry of the thermosphere mass density during the geomagnetic storm. Densities observed by satellite TM02 at nearly 11.3 and 23.3 LTs were larger in the northern hemisphere than in the southern. The TM04 dayside density observations appear to be almost symmetrical with respect to the equator, though southern hemisphere densities on the nightside were higher. Swarm-B data exhibit near-symmetry between the hemispheres. In addition, the mass density ratio results show that TM04 nightside observations, TM02 data, and Swarm-B data all clearly show stronger effects in the southern hemisphere, except for TM04 on the dayside, which suggest hemispheric near-symmetry. The South-North density enhancement differences in TM02 and TM04 on dayside can reach 130%, and Swarm-B data even achieve 180% difference. From the observations of all three satellites, large-scale traveling atmospheric disturbances (TADs) first appear at high latitudes and propagate to low latitudes, thereby disturbing the atmosphere above the equator and even into the opposite hemisphere. NRLMSISE00 model simulations were also performed on this geomagnetic storm. TADs are absent in the NRLMSISE00 simulations. The satellite data suggest that NRLMSISE00 significantly underestimates the magnitude of the density response of the thermosphere during geomagnetic storms, especially at high latitudes in both hemispheres. Therefore, use of the density simulation of NRLMSISE00 may lead to large errors in satellite drag calculations and orbit predictions. We suggest that the high temporal and spatial resolution of direct density observations by the TM-1 constellation satellites can provide an autonomous and reliable basis for correction and improvement of atmospheric models.

Keywords: TM-1 constellation; Swarm-B; joint observations; geomagnetic storm; Local Times

1. Introduction

TM-1 (TianMu-1) is the first satellite constellation from China — and perhaps even in the world — to conduct in situ detection of the neutral atmospheric mass density and composition of the thermosphere near 500 km. Mass density and composition are two crucial parameters in the thermosphere at altitudes of 80 to 1000 km. Mass density, correlated with satellite drag force, plays a vital role in the lifetime and orbit maintenance of low Earth orbit (LEO) spacecrafts in the thermosphere (Kim et al., 2006; Oliveira et al., 2020). The neutral composition of the thermosphere determines the free atmosphere average molecular mass associated with scale height that reflects the local mass density. Moreover, thermosphere density and composition are of great significance

Correspondence to: Y. P. Li, lyp@nssc.ac.cn
Received 13 JUL 2023; Accepted 28 OCT 2023.
First Published online 29 DEC 2023.

in the study of electrodynamic and photochemical ionosphere-thermosphere coupling processes.

The thermosphere density is mainly affected by solar extreme ultraviolet radiation, particle precipitation, and Joule heating (Xu JY et al., 2015; Zhang B et al., 2012; Wang X et al., 2022). Especially, Joule heating accounts for two-thirds of the energy injected into the high latitudes of the thermosphere during geomagnetic storms, which in turn leads to an increase in mass density (Cai L et al., 2014). Furthermore, Wang X et al. (2020) statistically analyzed the characteristics of Joule heating distribution under different levels of geomagnetic activity, and its influence on thermosphere density, by using the measurement results obtained by Challenging Minisatellite Payload (CHAMP) and Gravity Recovery and Climate Experiment (GRACE). The results show that peak duration of Joule heating is proportional to the intensity of a geomagnetic storm. Many past studies have shown hemispheric asymmetry, manifested as density enhancements in high latitude regions during geomagnetic storms (Bruinsma et al., 2006; Ercha et al., 2012; Li YP et al., 2023). Analysis of data collected during the geomagnetic storm event on 8 September 2017 showed that the density response amplitude of the southern polar region was 1.33–1.65 times that of the northern polar region (Ai JZ et al., 2023). Asymmetry of plasma convection between the hemispheres causes hemispheric differences in Joule heating at high latitudes, which is an important reason for the hemispherical difference of density response during a disturbance (Hong Y et al., 2021). Hemispheric asymmetry of density enhancements is also associated with local time (LT) differences. Li RX and Lei JH (2021) found that the density enhancement was almost hemispheric-symmetrical around 8–10/20–22 LT, whereas the southern hemisphere enhancement was stronger at 16 LT.

Traveling ionospheric disturbances (TIDs) and their neutral counterpart, traveling atmospheric disturbances (TADs), are important physical phenomena in the thermosphere. TADs represent a mechanism for global redistribution of energy and momentum in the thermosphere associated with magnetic storms and auroral substorms; understanding them is critical to understanding solar-terrestrial coupling (Bruinsma and Forbes, 2007). However, limited in situ observations have made it difficult to determine the sources, characterization, and evolution of TADs (Bruinsma and Forbes, 2009). Although modeling work has been widely performed (Lei JH et al., 2010; Deng Y et al., 2013; Lu G et al., 2016) and produced more consistent neutral density enhancements, the transient properties and time scales of TADs and the related perturbations place high demands on the model. Joint observations by multiple satellites are one possible detection means to achieve the high spatiotemporal resolution that is necessary. Li RX and Lei JH (2021) used density data from GRACE, Swarm-A, and Swarm-B satellites, which were at different altitudes, to discover the location and propagation characteristics of TADs.

In our study, we make full use of the detection advantages of the TM-1 constellation at the same altitude but different Lts. We have combined TM-1 data with Swarm-B observations to compare the response characteristics of the thermosphere atmosphere around 500 km during the geomagnetic storm event in April 2023, including hemispheric response differences, and TAD generation locations and propagation. We have then compared these detailed empirical observations to the performance of NRLMSISE00 simulations of this magnetic storm event.

2. Satellites Description

2.1 TM-1 Constellation

The TM-1 constellation will consist of 12 identical microsatellites evenly distributed in the sun-synchronous orbital plane at six different places with an inclination of 97° and altitude of about 500 km. The descending nodes of each orbital plane are: 7:20 LT, 9:40 LT, 11:30 LT, 13:10 LT, 15:30 LT, and 17:50 LT. The in-situ atmospheric payload carried by TM-1 satellites includes Atmospheric Density Detectors (ADD) and Atmospheric Composition Detectors (ACD); these detectors make possible global atmospheric exploration covering multi-orbital planes, collecting globally distributed, all-weather thermosphere atmospheric key parameters. The satellites' spatial layout of atmospheric in-situ detection is shown in Table 1. Except for the 13:10 LT orbital plane layout with two ACDs, satellites in other orbital planes are to be equipped with ADDs, which measure the total mass density. At the time of the work reported here, there were 6 satellites in orbit, distributed in the two orbital planes of 11:30 and 15:30 LT; two satellites arranged in the 11:30 LT plane were successfully launched on January 9, 2023, followed by four satellites launched into the 15:30 LT plane on March 22. Launches of satellites in other orbital planes were scheduled to be completed in 2023. The difference in latitude phase between satellites for each LT plane is also shown in Table 1.

Table 1. Spatial distribution of TM-1 constellation for thermosphere atmosphere in situ detections (* denotes launched).

Descending node (LT)	Satellites number	On-board instrument	Satellite layout (Latitude difference)
07:20	1	ADD	–
09:40	2	ADD	180°
11:30*	2	ADD	180°
13:10	2	ACD	180°
15:30*	4	ADD	90°
17:50	1	ADD	–

In this study, mass density data collected in situ by the ADD aboard one satellite from each of the 11:30 and 15:30 LT planes are evaluated and analyzed. The two satellite are named "TM02" and "TM04" respectively. The total mass density detection principle of the ADD is based on the theory of free atmosphere molecular dynamics, calculated by directly measuring gas pressure and gas temperature in the sampling chamber. The sampling chamber pressure resolution of the ADD is 1 Hz; the corresponding atmospheric mass density observation error is better than 10%; the measurement range is from 5×10^{-14} to 1×10^{-11} kg/m^3, which is wide enough to cover the mass density variation in the different space environments around 500 km. The TM02 and TM04 in situ data used in this paper are linear calibration processing of density data obtained based on the Two-Line Elements (TLE) method

inversion; for specific operation procedures, refer to Li X et al. (2018).

2.2 Swarm Constellation

The Swarm constellation consists of three satellites, Swarm-A, Swarm-B, and Swarm-C; they entered near-polar orbits on November 22, 2013, with an average altitude of about 510 km above the Earth's surface. During the first three months of 2014, the altitudes of Swarm-A and Swarm-C were reduced to about 480 km by orbital control, and Swarm-B was raised to about 530 km, eventually reaching a preset orbital altitude. Each Swarm satellite carries a GPS receiver and accelerometer. The GPS receiver can be used to determine non-gravitational forces acting on the spacecraft, such as drag and radiation pressure. Accelerometers measure these forces directly with much finer resolution than GPS receivers. Both payloads can yield the thermosphere atmospheric mass density. However, the acceleration measurement is subject to various influences, especially in the case of Swarm-B, which has a low signal-to-noise ratio; due to its high altitude and large noise, its accelerometer data are not available (Siemes et al., 2016). But Calabia et al. (2015) and Li RX et al. (2017) have shown that atmospheric mass density data inverted by GPS receivers is a good substitute when accelerometer data are missing. Considering that only Swarm-B of the three Swarm satellites is close to the TM-1 constellation orbit, only it is suitable for joint observations of thermosphere atmospheric mass density with TM-1 satellites; therefore, we use Swarm-B's Precise Orbit Determination (POD) data from its GPS receiver in the analysis presented in this paper.

3. Result

3.1 Satellites Location during 23–24 April 2023

Figure 1 shows the spatial distribution of TM02, TM04, and Swarm-B satellites during April 23–24, 2023. It can be seen from Figure 1a–b that the orbital distribution of the three satellites is relatively uniform, and the LT of descending nodes are at 11.3 h, 15.5 h and 19.8 h respectively. The LT difference between the ascending or descending branches is about 4 h. In addition, the orbital altitude of all three satellites is about 510 km during April 23–24. Therefore, this provides a good opportunity to analyze the thermosphere atmospheric response characteristics when multiple satellites are at the same altitude but different LTs at the time of a geomagnetic storm.

3.2 Mass Density Response Analysis

Figure 2 displays the variations of thermosphere mass density, solar wind, and geomagnetic parameters during the geomagnetic disturbance on April 23–24, 2023. This geomagnetic disturbance event was the strongest geomagnetic storm since the 25th solar cycle. The direct cause of the geomagnetic storm was the arrival at Earth of a coronal mass ejection from the solar eruption of April 21. According to the changes of geomagnetic index *Kp* and *Dst*, the disturbance events on April 23–24 can be divided into three parts: (i) the geomagnetic quiet period from 00:00 to 12:00 UT on the 23rd; (ii) the geomagnetic main phase from 12:00 on the 23rd to 06:00 UT on the 24th and (iii) the recovery phase after 06:00 UT on the 24th. The thermosphere mass density includes the observations and the corresponding density values normalized to 510 km, as shown in Figure 2a–c. The purpose of the normalization operation is to eliminate errors due to changes in orbital altitude by the following method (Picone et al., 2002; Bruinsma et al., 2006):

$$\rho(510\ \text{km}) = \rho(h) \times \frac{\rho_{\text{MSIS}}(510\ \text{km})}{\rho_{\text{MSIS}}(h)}, \tag{1}$$

where $\rho(510\ \text{km})$ stands for the density value normalized to 510 km, $\rho(h)$ is the original observation along the track; Correspondingly, ρ_{MSIS} is the NRLMSISE00 model value.

For the quiet period, the solar and geomagnetic activity is weak, which is reflected in the plasma velocity of about 350 km/s (Figure 2e) and the maximum *Kp* of 3 (Figure 2g). There is no significant change in the mass density recorded at the three satellites during this phase, except for the harmonic effects of solar insolation. The normalized density values are also largely consistent with the original observations. However, the normalized density values of TM04 have significantly amplified peaks in orbital circles 7 and 8 (see Figure 2b). In the early stage of the main phase of the magnetic storm (12:00–16:00 UT), *Dst* is slowly decreasing while

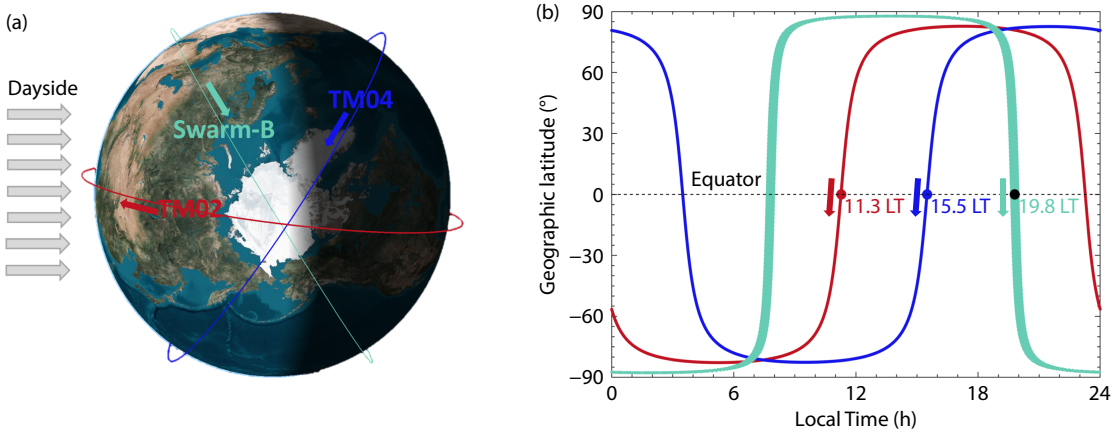

Figure 1. Relative spatial positions of TM02 (red line), TM04 (blue line), and Swarm-B (green line) during April 23–24, 2023. (a) Three-dimensional global orbit from perspective of the North Pole; (b) Geographic latitude versus Local Time. The colored arrows indicate the moving direction of the corresponding satellite.

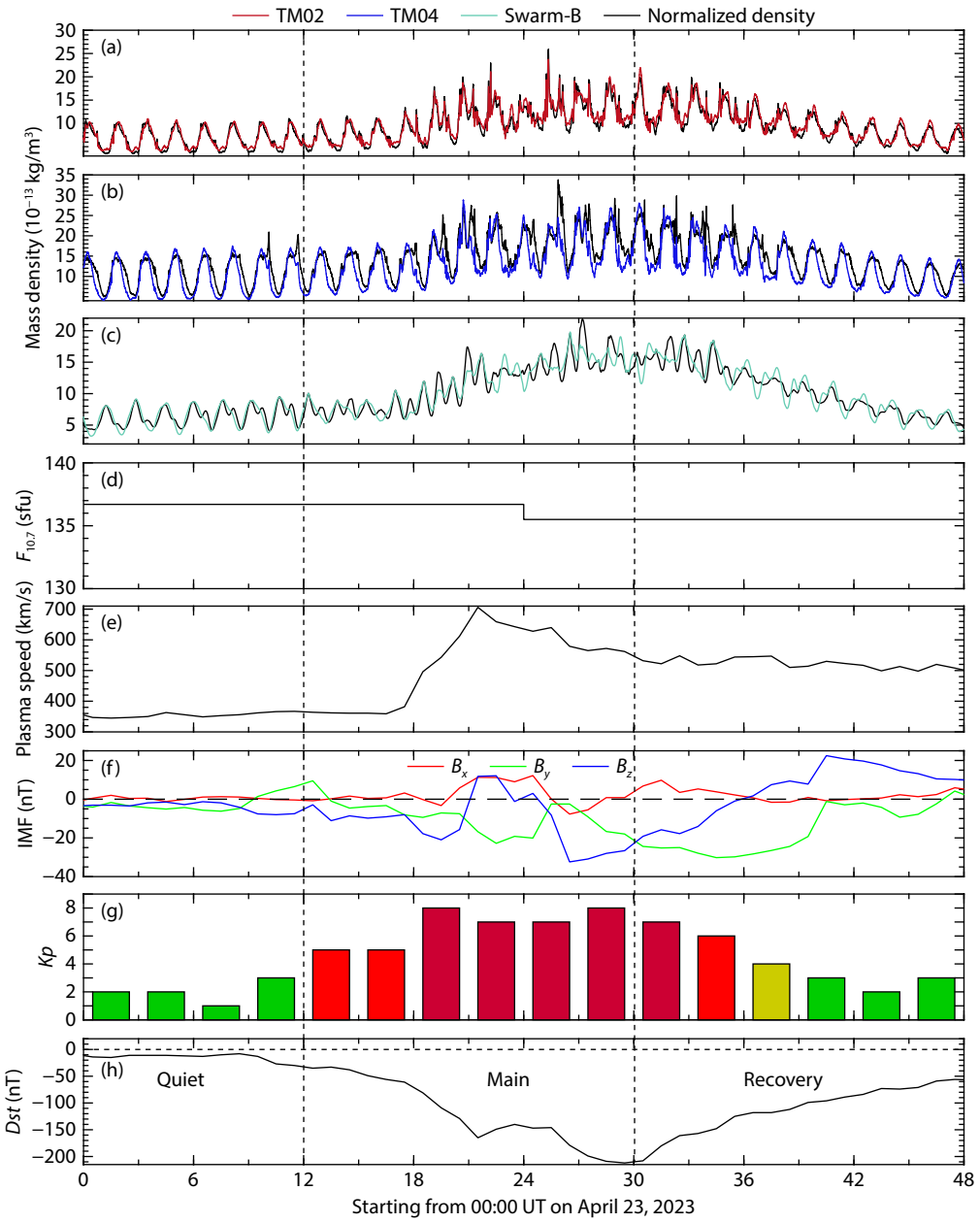

Figure 2. Thermosphere mass density variations during the geomagnetic disturbance on April 23–24, 2023. (a) The red line indicates TM02 observations; (b) TM04 data are represented by the blue line; (c) Turquoise denotes Swarm-B POD data; (d) Solar radiation index $F_{10.7}$ in sfu; (e) Plasma Speed outside the magnetosphere; (f) Three components of the interplanetary magnetic field in GSM coordinates, B_x (red), B_y (green), B_z (blue); black dash line means $|B| = 0$; (g) *Kp* index; (h) Geomagnetic index *Dst*. The black lines in (a), (b), and (c) represent the corresponding normalized mass density values.

Kp increases to 5, accompanied by a small disturbance in the atmospheric mass density of the thermosphere. Then the plasma velocity suddenly increases sharply from 350 km/s to 700 km/s, indicating that the magnetosphere is compressed more violently. *Kp* and *Dst* come to extremes of 8 and −165 nT, respecively, near 19:30 UT and then both retreat. Because the interplanetary magnetic field B_z turns from south to north (Figure 2f), it slightly weakens the energy and momentum conversion at the magnetopause. Immediately afterwards, B_z drops rapidly (within a few hours) to −32 nT while *Dst* reaches a minimum of −208 nT and geomagnetic activity reaches its maximum. In the main phase (severe geomagnetic disturbance), the mass densities measured at TM02, TM04, and Swarm-B increase significantly, and the density "valley" caused by the north direction of B_z can also be seen. The normalized density detected at TM02 during the main phase of the magnetic storm is basically consistent with the original observations. Compared with the original value, the normalized densities from data collected by TM04 and Swarm-B are slightly increased. After about 18 hours, the thermosphere mass density values drop to a level close to that detected before the disturbance. Overall, the normalized values retain the original density structure. Besides, the solar radiation index $F_{10.7}$ remains around 136 during the whole magnetic storm, so the disturbance variations in mass density are related only to geomagnetic activity.

TM04 data exhibit a higher ratio of peak to valley of mass density than TM02 data, and Swarm-B data exhibit the smallest ratio; these ratios are indicative of the intensity of solar insolation received at each satellite's orbit.

Figure 3 shows the variations with geographic latitude and UT in thermosphere mass density, as observed from TM02, TM04, and Swarm-B in their descending and ascending branches. The mass density has been normalized to a constant altitude of 510 km based on Equation (1), and grid averaged. From Figure 3, it can be noted that TM04 registered a greater mass density than TM02 and Swarm-B throughout the geomagnetic storm phase, because TM04 orbits on the afternoon side, where the atmosphere is more heated by solar radiation. When magnetic storms come, the mass density in the high latitudes of the northern and southern hemispheres is affected almost simultaneously and increases to about 21.7×10^{-13} kg/m^3 (see Figure 3b). This density disturbance response even impacts on the full latitude range. Meanwhile, results from the afternoon side of TM04 show a distinct feature: a significant density enhancement near 70°S at 12:00 UT. This phenomenon was also explained in the previous analysis; normalization of the density of this region increases its apparent enhancement level. However, the primary causes of this density enhancement in the polar cusp on dayside are field-aligned current heating (Neubert and Christiansen, 2003) and soft particle precipitation (Zhang B et al., 2012). Figure 3e shows the strong hemisphere asymmetry of the density values of TM04 during its ascending branch: The magnitude and latitude range of density disturbances in the southern hemisphere are significantly larger than in the northern hemisphere. In high latitudes, the southern hemisphere density value is about 1.2 times that in the same latitudes of the northern hemisphere. The peak of the southern hemisphere density disturbance region extends from 80°S to 30°S, while the northern hemisphere density disturbance seems to be confined to latitudes above 70°N. In addition, at 24 UT in Figure 3b, there is a density peak "trough" in the region from the high latitudes of the northern hemisphere to the low latitudes of southern hemisphere, which is consistent with the previous analysis of B_z northward. Figure 3a displays the TM02 ADD-based mass density in the forenoon (around 11.3 LT); in the northern hemisphere, three density-enhanced regions at high-latitude (around 80°N) were observed at about 22, 26, and 32 UT, respectively. The first two have an approximate density magnitude of 21.5×10^{-13} kg/m^3; the third is smaller, at 17.8×10^{-13} kg/m^3. Similarly, TADs can be observed in the southern hemisphere. But the maximum density value (19.5×10^{-13} kg/m^3) is smaller than in the northern hemisphere. The time of appearance of a mass density disturbance in low latitude regions of the thermosphere is related to the latitudinal propagation of TADs generated at high latitude; the lag in such cases is about 3 hours. Previous studies (Fujiwara and Miyoshi, 2006; Bruinsma and Forbes, 2007) have shown that the propagation speed of TADs is in the range of 300 to 800 m/s; thus it takes several hours at this speed for TADs to travel from the polar region to the equator, which is consistent with the observations presented in Figure 3.

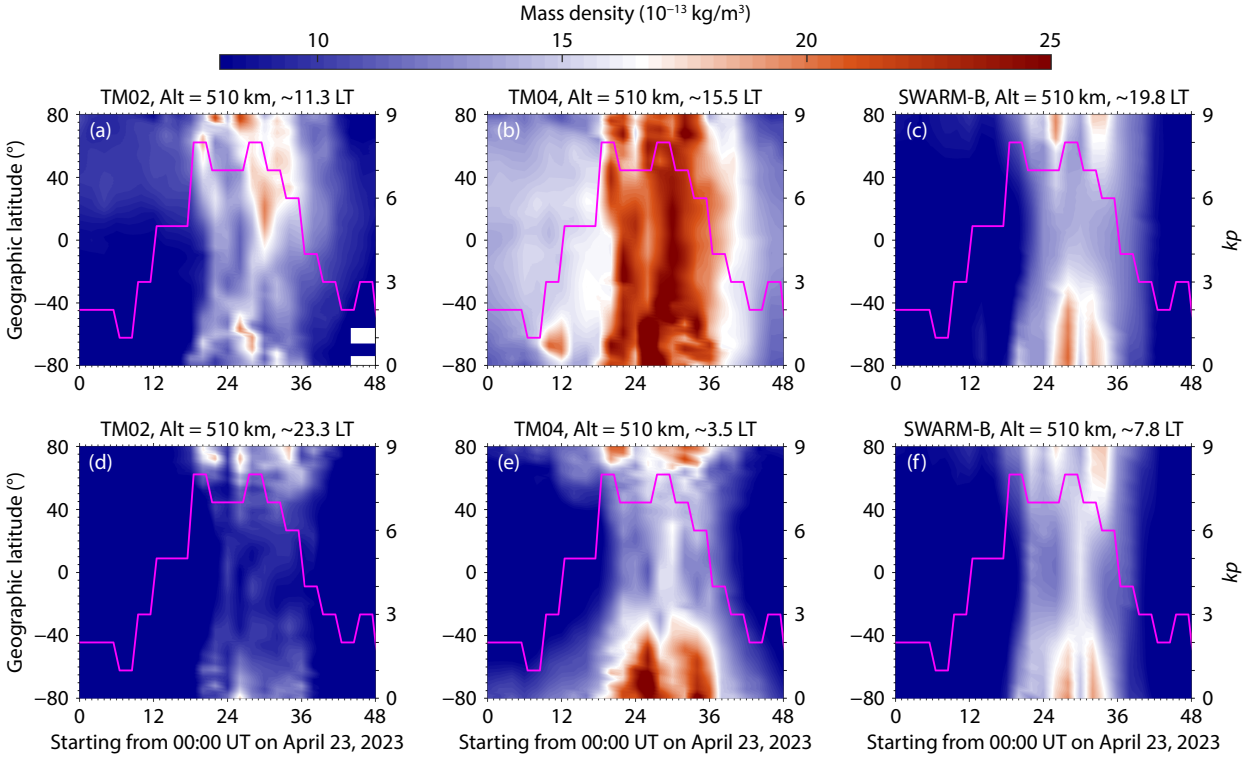

Figure 3. The mass density normalized to 510 km versus geographic latitude and UT during April 23–24, 2023. (a) and (d) are observations of TM02/ADD around 11.3 and 23.3 LT, respectively; (b) and (e) are separately derived from TM04/ADD around 15.5 and 3.5 LT; (c) and (f) are obtained from Swarm-B/POD around 19.8 and 7.8 LT. In addition, the magenta line of each subplot represents the geomagnetic index *Kp*, and the color scale is unified.

TM02-measured mass densities in the nightside are shown in Figure 3d. Overall, nightside absolute densities are lower than dayside values, which again is consistent with our basic understanding of the thermosphere atmosphere. Like the dayside display, nightside TADs are generated also in the high latitudes of both hemispheres. The difference is that TADs on the nightside move longer to low latitudes and the equator than on the dayside, their effects in low latitudes and the equator lasting for about 14 hours. At the same time, it can also be seen that densities in the northern hemisphere during the main phase are greater than those in the southern hemisphere.

Densities derived from POD data (shown in Figure 3c and f) are used to compare the thermosphere mass density response characteristics at different LTs during the geomagnetic storm. Since the POD data have temporal resolution of 30 s, which is lower than that of the TM-1 constellation ADD data (1 s), Swarm-B's POD density data appear smoother in structure and may seem even to have no detailed structure. As shown in Figure 3c, the high latitude regions of both hemispheres exhibit two TADs, with intensities of 19.5×10^{-13} kg/m^3 at approximately 26 UT, and 17.5×10^{-13} kg/m^3 at 33 UT. Similarly, X–shaped TADs (Qian LY et al., 2019) appear in the morning sector; this structure of "X-shaped TADs" indicates a global redistribution of energy and momentum in the thermosphere during magnetic storms. The absolute mass densities recorded by Swarm-B, located on the dawn/dusk side, are symmetric, and thus different from the characteristics of the north high and south low density distributions recorded by TM02. This difference calls attention to how a TAD affects thermospheric density at 510 km, as a function of LT.

Figure 3 shows the absolute mass density response of the thermosphere during a large geomagnetic storm, but it is important to note that the pre-storm densities of the two hemispheres differ. Therefore, to quantify the magnitude of density enhancement caused by the storm, we calculate the mass density ratio over the whole storm, as shown in Figure 4. The method used to obtain the mass density ratio is $(\rho_{storm} - \rho_{quiet})/\rho_{quiet}$, where ρ_{quiet} is the mean density at each latitude during the quiet period. From the overall distribution, the three satellite observations show that the ratio of mass density increase in the southern hemisphere was higher than that in the northern hemisphere. Moreover, Swarm-B recorded the largest peak density ratio; TM02 and TM04 density ratios were similar to each other. However, all three indicate that the thermosphere density response is still different at diverse LTs. Swarm-B's storm-induced density ratio peaks extend from the southern hemisphere to the equator (Figure 4c) and even into the northern hemisphere (Figure 4f). Figure 4b shows that the hemispheric density enhancement recorded at TM04 is almost symmetrical during the main phase, except around 26 UT. Unlike the TM04 dayside phenomenon, the peak density disturbance recorded at TM02 near 11.3 LT (Figure 4a) is mainly concentrated above 40°S in the southern hemisphere. The peak density ratio on the nightside affected the global latitude range in this magnetic storm, as shown in the Figure 4d, which is similar to the nightside density behavior observed by TM04. However, the high latitude density response characteristics recorded in the forenoon (Figure 4a) indicate that the southern hemisphere response is several hours earlier than that in the northern hemisphere; this is opposite to what was observed in the nightside by TM04.

All in all, by comparing the relative density response characteristics derived from data collected by TM02, TM04, and Swarm-B during

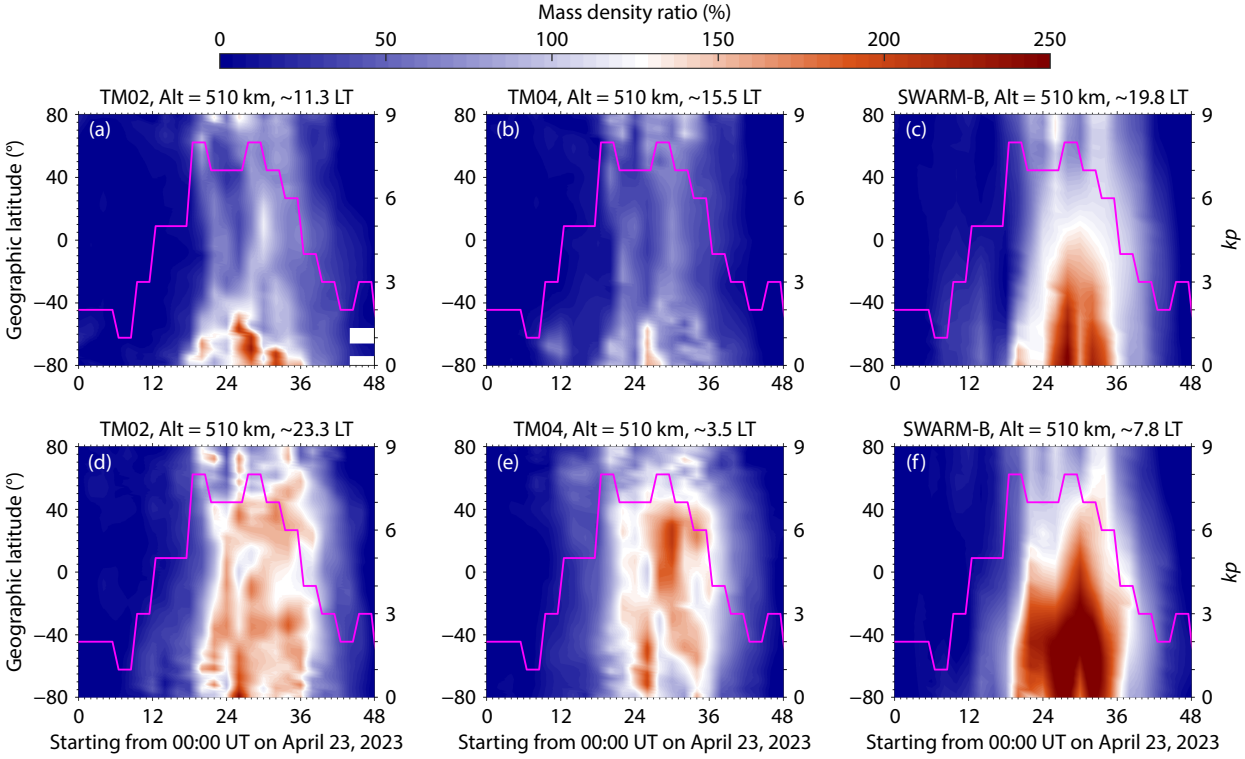

Figure 4. Same as Figure 3, except for the mass density ratio.

the geomagnetic storm, the TM04 results around 15.5 LT show that the density enhancements in the two hemispheres were almost symmetrical with respect to the equator. However, the nightside density enhancements derived from these data appear stronger in the southern hemisphere than in the northern. The South–North enhancements difference observed by TM02 and in the nightside by TM04 can reach 130%; the Swarm-B observations are even more asymmetric — a difference of 180%. This hemispheric response difference may be related to differences in energy deposition and propagation of perturbations. During geomagnetic storms, Joule heating is the dominant form of thermosphere energy deposition at high latitudes; it has been found that, in more intense geomagnetic storms, LT of peak density enhancement is closer to peak Joule heating LT (Wang X et al., 2021).

3.3 Comparison with the NRLMSISE00 Model

In this subsection, we examine NRLMSISE00, an internationally-used atmospheric empirical model, to simulate the thermosphere density response observed by TM02, TM04, and Swarm-B and compare model results with those from satellite data. The NRLMSISE00 mass densities are calculated along the orbits of TM02, TM04, and Swarm-B at their density sampling times and are performed identically as were the satellite observations. The results are presented in Figure 5, using the same density range color scale as in Figure 3. The NRLMSISE00 model simulation results differ significantly from the observed results in the following several ways: First, an obvious feature is that the NRLMSISE00 model underestimates the magnitude of the density response of the thermosphere observed during this geomagnetic storm, especially in the high latitudes (above 70°) of both hemispheres. For example, at a position around 80°N at 26 UT, the observed forenoon value from TM02 data is about 1.4 times the value computed by the NRLMSISE00 model (compare Figures 3a and 3d to Figures 5a and 5d). The model's simulation compared to data from TM04 is underestimated by about 50%. This suggests that the NRLMSISE00 model underestimates Joule heating in the high-latitude region of the thermospheric atmosphere. Second, none of the NRLMSISE00 simulations capture the time lag, actually observed in the satellite data, between the time of the high-latitude storm and the appearance of low-latitude density disturbances. As shown in Figures 5c and 5f, when the geomagnetic storm occurs, the Swarm-B model simulation predicts an almost simultaneous density response across the full latitude range. Third, the NRLMSISE00 simulations lack the richness of detail of the observed density structure; they do not even suggest this aspect of the phenomenon. For instance, Figure 3b (based on TM04 data) shows significantly enhanced density at 12 UT in the mid- and high-latitude regions; Figure 5b (the corresponding NRLMSISE00 simulation) totally lacks this detail, indicating that the NRLMSISE00 model fails to track what happens after energy injection in the dayside polar cusp. These differences strongly suggest that NRLMSISE00 has obvious disadvantages in simulating thermosphere density, especially in the case of space environment disturbances.

The generation and propagation of TADs and their local time characteristics are of great current interest to researchers trying to understand the thermospheric atmosphere, especially the electrodynamic process of magnetospheric–ionosphere–thermosphere

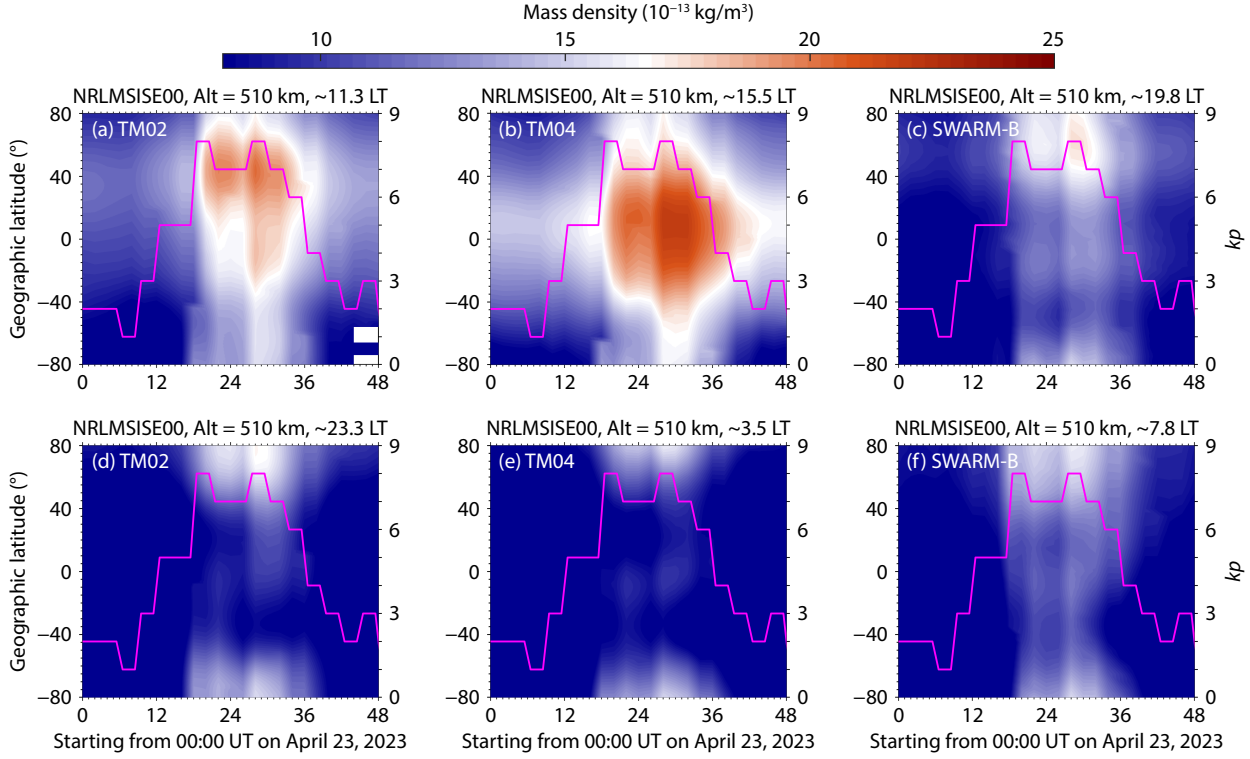

Figure 5. Consistent with the presentation shown in Figure 3, the results of the NRLMSISE00 empirical simulations are shown here: in time and space with the observations of the corresponding satellites, averaged on a grid.

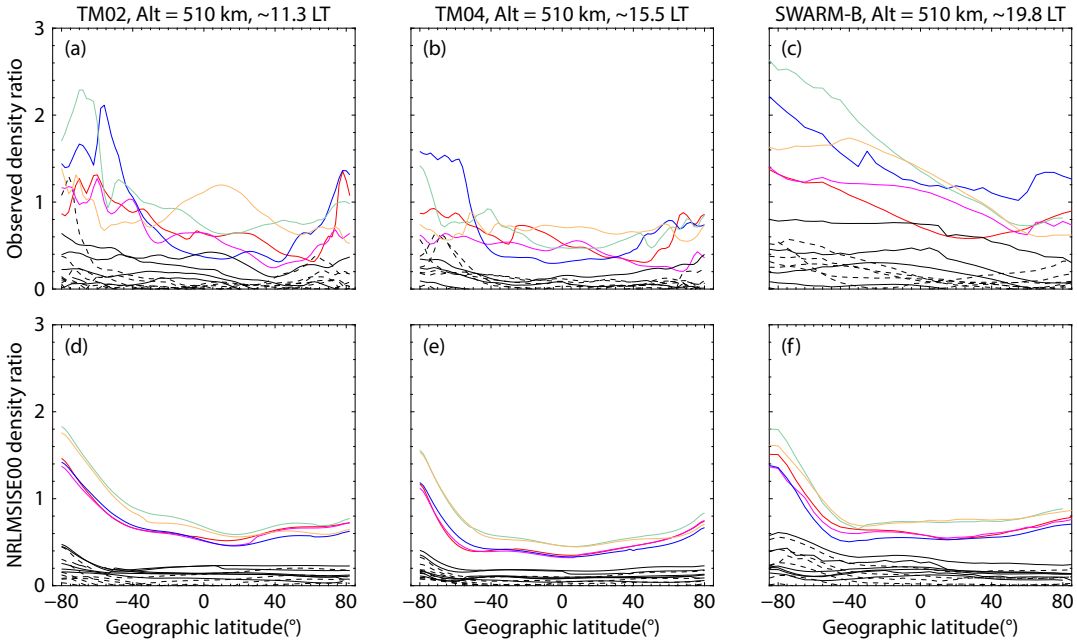

Figure 6. Mass density ratios at 510 km, derived from data collected by TM02 (near 11.3 LT), TM04 (around 15.5 LT), and Swarm-B (about 19.8 LT), are seen to vary with latitude. The first row (a, b, c) are observed values; the second row (d, e, f) are NRLMSISE00 model simulations results corresponding to the satellite observations. The dashed black line and solid black line of each subplot represent periods of quiet and recovery, respectively. The colored lines are observed (simulated) values during the main phase of the magnetic storm. The red line corresponds to 22:00 UT on April 23. Each of the succeeding four lines, in the order of magenta, blue, green, and yellow, represents conditions two hours later than those at the time of the preceeding line.

coupling (Bruinsma and Forbes, 2007; Pham et al., 2022). Figure 6 illustrates that the mass density ratios derived from TM02, TM04 and Swarm-B data vary with latitude at 510 km and different LTs. The black dotted line denotes the quiet period before the disturbance. The colored curves represent periods of perturbation; the black line represents the recovery period after disturbance. TM02 mass density ratio observations at 11.3 LT (Figure 6a) show that large-scale TADs were first generated in the polar region (red line); then this density disturbance continued to strengthen due to the continuous injection of energy and momentum into the high latitude region of the thermosphere, and formed TADs around 70°S and 55°S (blue line), respectively, after which the intensity of the first TADs increased to about 2.3, the other weakened to 1.2 and continued to move towards low latitudes (green line), and finally formed a larger wave-like structure near the equator at 10°N as indicated by the yellow line. Similar to TM02, TM04 data also describe large-scale TADs and their propagation to lower latitudes. However, Figure 6c shows that Swarm-B observations are too smooth, and reveal basically no wave-like TADs, although they do indicate that the density ratio of the northern and southern hemispheres has increased significantly. Similarly, the corresponding NRLMSISE00 model simulation results show that no TADs appear. In summary, during magnetic storms, the NRLMSISE00 simulation results exhibit significant deficiencies in density intensity, detailed structure, and large-scale TADs; Swarm-B POD data, too, appear unable to describe the exact structure, due to their time resolution limitations. Conversely, the observations of TM02 and TM04 perform better in these areas. In particular, these early observations suggest that it is very likely there will be a more detailed description of the atmospheric mass density and atmospheric composition of the thermosphere when the ADD and ACD of other LTs (Table 1) are laid out in 2023.

4. Summary

TM-1 is the first constellation in China and the world to carry out in situ detection of the thermosphere neutral atmosphere, and to conduct joint observations on mass density and composition. In this study, the thermosphere mass density response during the April 23–24, 2023 geomagnetic storm was analyzed in detail using data derived from TM02, TM04 and Swarm-B satellites, and the simulation results of NRLMSISE00 were compared. During this magnetic storm, the three satellites were in orbit at different LT but at the same altitude. The LT difference between the ascending or descending branches of the three satellites is about 4 h. Therefore, this was a good opportunity to study the LTs properties of thermosphere density response. The main conclusions are summarized below:

(1) The observed results show that there were LTs differences in the hemispheric asymmetry of the thermosphere mass density during the geomagnetic storm in April 2023. TM02 density was larger in the northern hemisphere than southern hemisphere at nearly 11.3 and 23.3 LTs. For the dayside of TM04, the density appears almost symmetry with respect to the equator, while density behavior shows that the southern hemisphere was is higher than the northern hemisphere at around 3.5 LT. The density recorded by Swarm-B in the morning and dusk presents as approximately symmetrical between north and south.

(2) Comparison of the mass density ratio response characteristics recorded by TM02, TM04, and Swarm-B during the geomagnetic

storm in April 2023, with the exception of the dayside of TM04, suggests that the mass density ratio in the two hemispheres was almost symmetrical with respect to the equator. Data from TM04 on nightside, from TM02, and from Swarm-B all clearly show stronger response in the southern hemisphere. Moreover, the South–North enhancements difference in TM02 and TM04 on the dayside can reach 130%, and Swarm-B data even show a 180% difference.

(3) From the observations of TM02, TM04 and Swarm-B, large-scale TADs first appear at high latitudes and move in zonal direction, causing disturbances to the thermosphere atmosphere at low latitudes and the equator. However, TADs did not occur in the NRLMSISE00 simulations. For the model simulation results, it is obvious that NRLMSISE00 underestimates the magnitude of the density response of the thermosphere during geomagnetic storms, especially at high latitudes (above 70°) in the southern and northern hemispheres. Density simulations can be underestimated by about 50% during geomagnetic storms.

The remaining TM-1 atmospheric in situ detection satellites will be launched in late 2023, and it is believed that the complex physical process of thermosphere atmospheric response during geomagnetic storms will have a clearer understanding.

Acknowledgments

We acknowledge National Space Science Center (NSSC) of the Chinese Academy of Sciences for their full support of our research work. We sincerely express our gratitude to the team members of the project that built the TM-1 constellation. This research was funded by the China Manned Space Program (Grant Y59003AC40), and TM-1 Constellation Atmospheric Density Detector (Grant E3C1162110). The space environment indices such as solar wind came from NASA OMNIWeb data (https://cdaweb.gsfc.nasa.gov/).

References

Ai, J. Z., Li, Y. P., Zhang, X. P., Xiao, C., Chen, G. M., Zheng, X. L., and Zhang, Z. L. (2023). Study on the hemispheric asymmetry of thermospheric density based on in-situ measurements from APOD satellite. *Atmosphere*, *14*(4), 714. https://doi.org/10.3390/atmos14040714

Bruinsma, S., Forbes, J. M., Nerem, R. S., and Zhang, X. L. (2006). Thermosphere density response to the 20-21 November 2003 solar and geomagnetic storm from CHAMP and GRACE accelerometer data. *J. Geophys. Res.: Space Phys.*, *111*(A6), A06303. https://doi.org/10.1029/2005JA011284

Bruinsma, S. L., and Forbes, J. M. (2007). Global observation of traveling atmospheric disturbances (TADs) in the thermosphere. *Geophys. Res. Lett.*, *34*(14), L14103. https://doi.org/10.1029/2007GL030243

Bruinsma, S. L., and Forbes, J. M. (2009). Properties of traveling atmospheric disturbances (TADs) inferred from CHAMP accelerometer observations. *Adv. Space Res.*, *43*(3), 369–376. https://doi.org/10.1016/j.asr.2008.10.03

Cai, L., Aikio, A. T., and Nygrén, T. (2014). Solar wind effect on Joule heating in the high-latitude ionosphere. *J. Geophys. Res.: Space Phys.*, *119*(12), 10440–10455. https://doi.org/10.1002/2014JA020269

Calabia, A., Jin, S. G., and Tenzer, R. (2015). A new GPS-based calibration of GRACE accelerometers using the arc-to-chord threshold uncovered sinusoidal disturbing signal. *Aerosp. Sci. Technol.*, *45*, 265–271. https://doi.org/10.1016/j.ast.2015.05.013

Deng, Y., Fuller-Rowell, T. J., Ridley, A. J., Knipp, D., and Lopez, R. E. (2013). Theoretical study: Influence of different energy sources on the cusp neutral density enhancement. *J. Geophys. Res.: Space Phys.*, *118*(5), 2340–2349. https://doi.org/10.1002/jgra.50197

Ercha, A., Ridley, A. J., Zhang, D. H., and Xiao, Z. (2012). Analyzing the hemispheric asymmetry in the thermospheric density response to geomagnetic storms. *J. Geophys. Res.: Space Phys.*, *117*(A8), A08317. https://doi.org/10.1029/2011JA017259

Fujiwara, H., and Miyoshi, Y. (2006). Characteristics of the large-scale traveling atmospheric disturbances during geomagnetically quiet and disturbed periods simulated by a whole atmosphere general circulation model. *Geophys. Res. Lett.*, *33*(20), L20108. https://doi.org/10.1029/2006GL027103

Hong, Y., Deng, Y., Zhu, Q. Y., Maute, A., Sheng, C., Welling, D., and Lopez, R. (2021). Impacts of different causes on the inter-hemispheric asymmetry of ionosphere-thermosphere system at mid- and high-latitudes: GITM simulations. *Space Wea.*, *19*(11), e2021SW002856. https://doi.org/10.1029/2021SW002856

Kim, K. H., Moon, Y. J., Cho, K. S., Kim, H. D., and Park, J. Y. (2006). Atmospheric drag effects on the KOMPSAT-1 satellite during geomagnetic superstorms. *Earth Planets Space*, *58*(6), e25–e28. https://doi.org/10.1186/BF03351968

Lei, J. H., Thayer, J. P., Burns, A. G., Lu, G., and Deng, Y. (2010). Wind and temperature effects on thermosphere mass density response to the November 2004 geomagnetic storm. *J. Geophys. Res.: Space Phys.*, *115*(A5), A05303. https://doi.org/10.1029/2009JA014754

Li, R. X., Lei, J. H., Wang, X. J., Dou, X. K., and Jin, S. G. (2017). Thermospheric mass density derived from CHAMP satellite precise orbit determination data based on energy balance method. *Sci. China Earth Sci.*, *60*(8), 1495–1506. https://doi.org/10.1007/s11430-016-9052-1

Li, R. X., and Lei, J. H. (2021). Responses of thermospheric mass densities to the October 2016 and September 2017 geomagnetic storms revealed from multiple satellite observations. *J. Geophys. Res.: Space Phys.*, *126*(1), e2020JA028534. https://doi.org/10.1029/2020JA028534

Li, X., Xu, J. Y., Tang, G. S., Chen, G. M., Man, H. J., Liu, S. S., and Li, Y. P. (2018). Processing and calibrating of in-situ atmospheric densities for APOD. *Chinese J. Geophys. (in Chinese)*, *61*(9), 3567–3576. https://doi.org/10.6038/cjg2018L0452

Li, Y. P., Sun, Y. Q., Zhang, X. G., Du, Q. F., Tang, X. C., Zheng, X. L., Ai, J. Z., Meng, X. G., Li, J., ... Wei, S. L. (2023). The preliminary result of orbital atmosphere detector on board spherical satellite. *Sci. Sin. Tech. (in Chinese)*, *53*(4), 615–621. https://doi.org/10.1360/SST-2022-0074

Lu, G., Richmond, A. D., Lühr, H., and Paxton, L. (2016). High-latitude energy input and its impact on the thermosphere. *J. Geophys. Res.: Space Phys.*, *121*(7), 7108–7124. https://doi.org/10.1002/2015JA022294

Neubert, T., and Christiansen, F. (2003). Small-scale, field-aligned currents at the top-side ionosphere. *Geophys. Res. Lett.*, *30*(19), 2010. https://doi.org/10.1029/2003GL017808

Oliveira, D. M., Zesta, E., Hayakawa, H., and Bhaskar, A. (2020). Estimating satellite orbital drag during historical magnetic superstorms. *Space Wea.*, *18*(11), e2020SW002472. https://doi.org/10.1029/2020SW002472

Pham, K. H., Zhang, B., Sorathia, K., Dang, T., Wang, W., Merkin, V., Liu, H., Lin, D., Wiltberger, M., ... Lyon, J. (2022). Thermospheric density perturbations produced by traveling atmospheric disturbances during August 2005 storm. *J. Geophys. Res.: Space Phys.*, *127*(2), e2021JA030071. https://doi.org/10.1029/2021JA030071

Picone, J. M., Hedin, A. E., Drob, D. P., and Aikin, A. C. (2002). NRLMSISE-00 empirical model of the atmosphere: Statistical comparisons and scientific issues. *J. Geophys. Res.: Space Phys.*, *107*(A12), SIA 15-1-SIA 15-16. https://doi.org/10.1029/2002JA009430

Qian, L. Y., Wang, W. B., Burns, A. G., Chamberlin, P. C., Coster, A., Zhang, S. R., and Solomon, S. C. (2019). Solar flare and geomagnetic storm effects on the thermosphere and ionosphere during 6-11 September 2017. *J. Geophys. Res.: Space Phys.*, *124*(3), 2298–2311. https://doi.org/10.1029/2018JA026175

Siemes, C., de Teixeira da Encarnação, J., Doornbos, E., van den Ijssel, J., Kraus, J., Pereštý, R., Grunwaldt, L., Apelbaum, G., Flury, J., and Holmdahl Olsen, P. E. (2016). Swarm accelerometer data processing from raw accelerations to thermospheric neutral densities. *Earth, Planets Space, 68*(1), 92.

https://doi.org/10.1186/s40623-016-0474-5

Wang, X., Miao, J., Aa, E., Ren, T. L., Wang, Y. X., Liu, J., and Liu, S. Q. (2020). Statistical analysis of Joule heating and thermosphere response during geomagnetic storms of different magnitudes. *J. Geophys. Res.: Space Phys.*, *125*(8), e2020JA027966. https://doi.org/10.1029/2020JA027966

Wang, X., Miao, J., Lu, X., Aa, E., Liu, J., Wang, Y. X., and Liu, S. Q. (2021). Latitudinal impacts of Joule heating on the high-latitude thermospheric density enhancement during geomagnetic storms. *J. Geophys. Res.: Space Phys.*, *126*(7), e2020JA028747. https://doi.org/10.1029/2020JA028747

Wang, X., Miao, J., Lu, X., Aa, E., Luo, B. X., Liu, J., Hong, Y., Wang, Y. X., Ren, T. L., ... Liu, S. Q. (2022). Using temporal relationship of thermospheric density with geomagnetic activity indices and Joule heating as calibration for NRLMSISE-00 during geomagnetic storms. *Space Wea.*, *20*(4), e2021SW003017. https://doi.org/10.1029/2021SW003017

Xu, J. Y., Wang, W. B., Zhang, S. R., Liu, X., and Yuan, W. (2015). Multiday thermospheric density oscillations associated with variations in solar radiation and geomagnetic activity. *J. Geophys. Res.: Space Phys.*, *120*(5), 3829–3846, https://doi.org/10.1002/2014JA02083

Zhang, B., Lotko, W., Brambles, O., Wiltberger, M., Wang, W., Schmitt, P., and Lyon, J. (2012). Enhancement of thermospheric mass density by soft electron precipitation. *Geophys. Res. Lett.*, *39*(20), L20102. https://doi.org/10.1029/2012GL053519